ASTFE
American Society
of Thermal and Fluids Engineers

9th Thermal and Fluids Engineering Conference (TFEC)
April 21–24, 2024
Partially online virtual and in person at Oregon State University, Corvallis, OR, USA

TFEC-2024-50751

MACHINE-LEARNED TURBULENCE MODEL FOR TOPOLOGY OPTIMIZATION-BASED HEAT EXCHANGER DESIGN FRAMEWORK

Mitansh Tripathi,[1] Botao Zhang,[2] Vysakh Venugopal,[2] Navaneeth Chandran,[2] Logan Ware,[3] Niloofar Sanaei,[3] Sam Anand,[2] Prashant Khare[1,*]

[1]Department of Aerospace Engineering, University of Cincinnati, Cincinnati, OH 45221–0070
[2]Department of Mechanical Engineering, University of Cincinnati, Cincinnati, OH 45221–0072
[3]Eaton Research Laboratory, Digital Design & Engineering, Eaton Corporation, Southfield, MI 48076

ABSTRACT

Due to limitations imposed by manufacturing processes, heat exchanger designs previously were composed of tubes and fins (and several variants of these two geometric shapes). Recent advances in additive manufacturing techniques have led to the use of multi-objective topology optimization (TopOpt) to generate ”organic” heat exchanger designs that satisfy mission-specific requirements. TopOpt-based heat exchanger design frameworks were initially developed assuming laminar flow. However, for a multitude of applications, the gaseous flow is often turbulent. The purpose of this paper is to develop a machine-learned (ML) model that can be incorporated into a TopOpt framework to design heat exchangers. Specifically, design inputs include domain size (10”$\times$ 10”), temperature, and flow rates of hot (80 ^{o} C, 11 L/min) and cold fluids (55 ^{o}C, 67 m/s) and constraints based on energy density, pressure loss, and manufacturability. The hot and cold fluids are an aqueous solution of 50-50 ethylene glycol and air, respectively. A ML-based turbulence model is developed by first simulating the flow and heat transfer on 10 preliminary heat exchanger designs using two-equation, realizable $\kappa - \epsilon$-based steady RANS (Reynolds-Averaged Navier-Stokes) calculations. Then, a Gaussian Process machine learning model is trained to calculate the turbulent viscosity using area density as the input variable. The model is validated by performing an RANS calculation using a 0-equation eddy viscosity model with the eddy viscosity predicted by the GP model and comparing it with the test data. The outlet temperatures of both calculations were within 2% of each other. The next step is to incorporate this model into the TopOpt framework.

KEY WORDS: organic heat exchangers, turbulence modeling, machine learning, Gaussian Process, topology optimization, additive manufacturing

1. INTRODUCTION

Heat exchangers are essential devices widely used in various industries to facilitate the transfer of thermal energy between two fluids while maintaining a clear separation between them through the use of a solid barrier. These devices find applications in scenarios such as engine cooling, refrigeration, and many others [1]. This paper specifically discusses heat exchangers involving two fluids in which there is no phase change involved, such as condensation or evaporation. In such heat exchangers, the primary mode of heat transfer is forced convection, which refers to the process in which the movement of fluids is driven by external means, such as pumps or fans, to enhance the transfer of energy from the hot fluid to the cold fluid. Analysis of such devices requires a coupled solution of the processes that govern the flow of the two fluids and the conduction

*Corresponding Prashant Khare: Prashant.Khare@uc.edu

of heat within the solids, which is also called conjugate heat transfer (CHT).

In a heat exchanger, energy from the hot coolant is convected to the inner surface, which is then conducted through the solid walls of the heat exchanger to its outer surface. Subsequently, the cold fluid convects the heat away from the outer surface. The coolant then recirculates to extract more energy from the component to be cooled.

Contemporary designs consist of relatively simple configurations such as shell and tube-type and fin and tube-type heat exchangers. The fin and tube designs represent the cutting edge in compact heat exchanger technology [2]. Various techniques have been explored to enhance their efficiencies, including altering the geometry of the fins, adjusting the spacing between components, or incorporating vortex generators. One such approach involves employing wavy fin arrangements to increase the surface area of the heat exchanger, resulting in a longer airflow path and facilitating extended interaction between the air and the heat exchanger. In another method, vortex generators are strategically placed on the fins to induce turbulence. This approach significantly enhanced the mixing, leading to enhanced heat transfer[2]. Numerous research efforts have been extensively documented in the literature to improve the efficacy of conventional heat exchangers [3–6].

It is well known that conventional heat exchangers are not the optimum designs to extract energy from a system; however, due to the constraints imposed by manufacturing processes (e.g. cost constraints of mass production), industries for most of the last century have relied on simple designs. However, recent advances in additive manufacturing techniques have the potential to revolutionize the design of heat exchangers. An emerging design technique, Design for Additive Manufacturing (DfAM) combined with multiobjective topology optimization (TopOpt), is increasingly being used to design components to achieve specific objectives, including the design of heat exchangers [7–11].

In the current research effort, we are developing two-fluid ”organic” heat exchanger designs using DfAM and TopOpt that maximize the heat extraction from the hot fluid, given the domain size, temperatures and flow rates of the two fluids, allowable pressure drop, weight and constraints imposed by the additive manufacturing processes. The word ”organic” refers to a situation where the shape of the heat exchanger is not known a priori. The process of getting a final topologically optimized design is to start with a black box and the final heat exchanger is built with each successive iteration. In essence, the Navier-Stokes equations become a part of the objective function, which generates heat exchanger designs for the given constraints using TopOpt based on density [12]. For the Reynolds numbers of interest, the hot fluid (a liquid) is in the laminar regime, whereas the cold fluid (air) is turbulent. A major challenge in the formulation is to model the turbulent flow of air as an objective function of the optimization algorithm. While there are sophisticated techniques to accurately model such flows such as direct numerical simulations [13] and large eddy simulations [14–16], to make TopOpt computationally tractable and ensure that it converges to a solution, closure based on Reynolds average Navier-Stokes (RANS) is adopted in the current algorithm. Among several RANS-based closure models, we use the zero-equation eddy viscosity model, which requires estimation of the turbulent viscosity μ_t. There are several ways to evaluate μ_t (e.g., mixing length) [17], however, since the geometry is not known, it is difficult to estimate it. To mitigate this issue, we use machine learning-based turbulence closure, the topic of discussion in this paper.

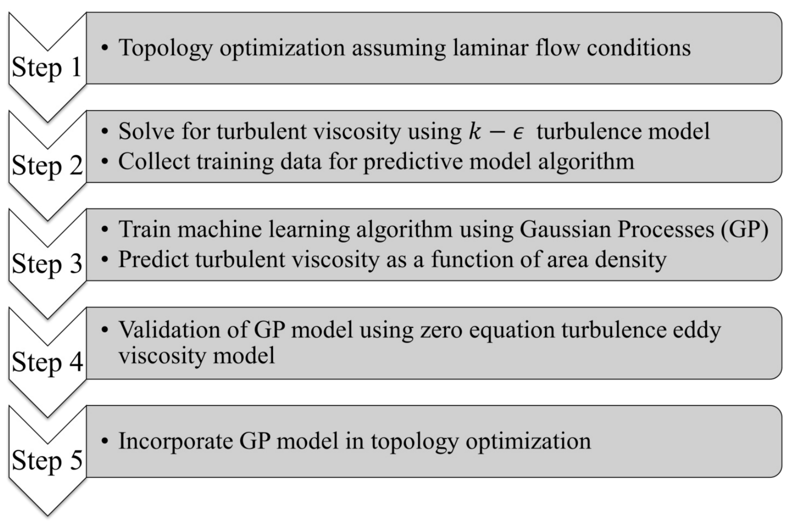

Fig. 1 Flowchart of the overall DfAM TopOpt framework.

For context, figure 1 shows the flow diagram of the overall algorithm. In the first step, several preliminary designs encompassing the operating envelope are generated assuming that both the hot and cold flows are laminar. These designs are then analyzed using the $k-\epsilon$ turbulence model. An outcome of this analysis is the spatially averaged turbulent viscosity and the corresponding area density in the domain of interest. Next, a Gaussian Process (GP) machine learning algorithm is trained which predicts the turbulent viscosity for a given area density. This model is then incorporated into the TopOpt algorithm to generate heat exchanger designs. Further details of the DfAM and TopOpt algorithms can be found elsewhere [18].

The rest of the paper is organized into four sections. Sections 2 and 3 detail the mathematical framework and experimental validation. Section 4 discusses the results, which include the process of generating the training data, the development of the machine-learned model, and the comparison between the ”truth” ($k-\epsilon$) and the flow physics predicted by the zero-equation RANS model that uses the turbulent viscosity predicted by ML at the test points. The main conclusions of the study are drawn in Section 5.

2. MATHEMATICAL FRAMEWORK

The equations governing the conservation of mass, momentum, and energy based on the incompressible form of the zero-equation RANS turbulence model that is used as the objective function in the TopOpt algorithm are summarized below.

$$\frac{\partial \bar{U}_i}{\partial x_i} = 0 \tag{1}$$

$$\rho \frac{\partial \bar{U}_i}{\partial t} + \rho \bar{U}_j \frac{\partial \bar{U}_i}{\partial x_i} = -\frac{\partial \bar{P}}{\partial x_i} + \frac{\partial}{\partial x_j}\left(2\mu S_{ji} - \rho \overline{u_j' u_i'}\right) \tag{2}$$

$$\frac{\partial \overline{T}}{\partial t} + \overline{U_j}\frac{\partial \overline{T}}{\partial x_j} = \frac{\partial}{\partial x_i}\left(\alpha \frac{\partial \overline{T}}{\partial x_i}\right) - \frac{\partial \overline{u_j' T'}}{\partial x_j} \tag{3}$$

Here $\overline{U}$ is the mean velocity vector, P the pressure, ρ the density, α the thermal diffusivity, and the quantity $\rho\overline{u_j' u_i'}$ is the Reynolds stress tensor. The strain rate tensor is given by $S_{ij} = S_{ji}$ and is given by

$$S_{ij} = \frac{1}{2}\left(\frac{\partial \bar{U}_i}{\partial x_i} + \frac{\partial \bar{U}_i}{\partial x_j}\right) \tag{4}$$

In a zero-equation, eddy viscosity-based turbulence model, the turbulent stress and other fluctuating components can be expressed in terms of turbulent viscosity (μ_t) given by:

$$\rho\overline{u_j' u_i'} = \mu_t \overline{S_{ij}} \tag{5}$$

$$\overline{u_j' T'} = \frac{\mu_t}{\rho Pr_t}\frac{\partial \overline{T}}{\partial x_i} \tag{6}$$

where μ_t is the turbulent viscosity and Pr_t is the turbulent Prandtl number, which is taken to be 0.9 based on standard values and justified by the turbulent theory [19]. There are several ways to estimate μ_t, which is the only term that needs to be closed. To be as accurate as possible and to eliminate the errors introduced by assumptions that underlie various closure models, we conducted ”higher” fidelity realizable $k-\epsilon$-based calculations using Star CCM+ and extracted turbulent viscosity (an output of the $k-\epsilon$ calculations) over the range of geometries of interest and trained a machine learning algorithm (discussed in Section 2.1 to predict the spatially averaged turbulent viscosity given a surface density that is used to close the last two terms of equations 2 and 3. The governing equations for the realizable $k-\epsilon$ [20] model are as follows:

$$\frac{\partial}{\partial t}(\rho k) + \frac{\partial}{\partial x_j}(\rho k u_j) = \frac{\partial}{\partial x_j}\left[\left(\mu + \frac{\mu_t}{\sigma_k}\right)\frac{\partial k}{\partial x_j}\right] + G_k + G_b - \rho\epsilon + S_k \tag{7}$$

$$\frac{\partial}{\partial t}(\rho\epsilon) + \frac{\partial}{\partial x_j}(\rho\epsilon u_j) = \frac{\partial}{\partial x_j}\left[\left(\mu + \frac{\mu_t}{\sigma_\epsilon}\right)\frac{\partial \epsilon}{\partial x_j}\right] + \rho C_1 S_{ij}\epsilon - \rho C_2\frac{\epsilon^2}{k+\sqrt{\nu\epsilon}} + C_{1\epsilon}\frac{\epsilon}{k}C_{3\epsilon}G_b + S_\epsilon \tag{8}$$

Here, G_k and G_b represent the production of turbulent kinetic energy due to mean velocity gradients and buoyancy, respectively. S_ϵ and S_k are user-defined source terms while $C_{1\epsilon}$ and C_2 are constants. $C_1 = max[0.43, \frac{\eta}{\eta+5}]$ where $\eta = S_{ij}\frac{k}{\epsilon}$. σ_ϵ and σ_k are turbulent Prandtl numbers for ϵ and k. Once the transport equations are solved, the turbulent viscosity is given by

$$\mu_t = \rho C_\mu \frac{k^2}{\epsilon} \tag{9}$$

The model constants are: $C_\mu = 0.09 \quad C_{1\epsilon} = 1.44 \quad C_2 = 1.9 \quad \sigma_k = 1.0 \quad \sigma_\epsilon = 1.2$ [17]. The computational domain comprises of three subdomains: air, EGW (50% ethylene glycol - 50% water), and aluminum, which is the material of choice for the heat exchanger. The Reynolds number corresponding to the flow of cold air is 7.28×10^5, while for EGW it is 3.07×10^3.

2.1 Gaussian Process Model

Gaussian Process (GP) is a Bayesian-based supervised learning approach. It is defined as a collection of random variables, any finite number of which has a joint Gaussian distribution [21]. It predicts an output y, given an input x based on n observations. The GP framework used in this research effort is based on our previous work on using GP to model spatiotemporal fluid dynamic processes [22, 23]. A GP model is specified by its mean and covariance functions given by:

$$f(x) \sim \mathcal{GP}(m(x), k(x, x')) \tag{10}$$

Where $m(x)$ is the mean function and $k(x, x')$ is the covariance matrix. The aim is to find a corresponding y_* value for a given input x_*. For this purpose, the covariance function is calculated as follows [21].

$$K = \begin{bmatrix} k(x_1,x_1) & k(x_1,x_2) & \cdots & k(x_1,x_n) \\ k(x_2,x_1) & k(x_2,x_2) & \cdots & k(x_2,x_n) \\ \vdots & \vdots & \ddots & \vdots \\ k(x_n,x_1) & k(x_n,x_2) & \cdots & k(x_n,x_n) \end{bmatrix} \tag{11}$$

$$K_* = [k(x_*,x_1) \quad k(x_*,x_2) \quad \cdots \quad k(x_*,x_n)] \quad K_{**} = k(x_*,x_*) \tag{12}$$

The desired output y_* is given by:

$$\begin{bmatrix} y \\ y_* \end{bmatrix} \sim \mathcal{N}\left(0, \begin{bmatrix} K & K_*^T \\ K_* & K - ** \end{bmatrix}\right) \tag{13}$$

Then the conditional probability $p(y_*|y)$, that is, the likelihood of the predicted value y_*, given all the data points y is given by the following expression:

$$y_*|y \sim \mathcal{N}(K_*K^{-1}y, \quad K_{**} - K_*K^{-1}K_*^T) \tag{14}$$

The predicted value, y_* and its variance is given by:

$$\overline{y_*} = K_*K^{-1}y \qquad var(y_*) = K_{**} - K_*K^{-1}K_*^T \tag{15}$$

Table 1 Operating conditions for the validation cases.

	Air	Water
Inlet velocity (m/s)	0.25, 0.36 and 0.46	0.76
Inlet temperature (^oC)	22	40

3. MODEL VALIDATION

To ensure that relevant flow physics and heat transfer mechanisms are captured, the realizable $k-\epsilon$-based calculations are used to simulate a conventional heat exchanger using Star CCM+ to assess the validity of the model and the underlying assumptions. Figure 2 shows that the configuration is based on the experiment conducted by Batista et al. [24], where a fin-and-tube heat exchanger was studied. The coolant used in the experiment is water that flows through 38 copper tubes which were attached to 260 aluminum fins perpendicular to the flow of water. The heat exchanger was placed in the test section of a wind tunnel, which provided a steady flow of air. Further details of the experimental setup are described in [24]. Three different cases with varying air velocities are conducted – the operating conditions are summarized in table 1.

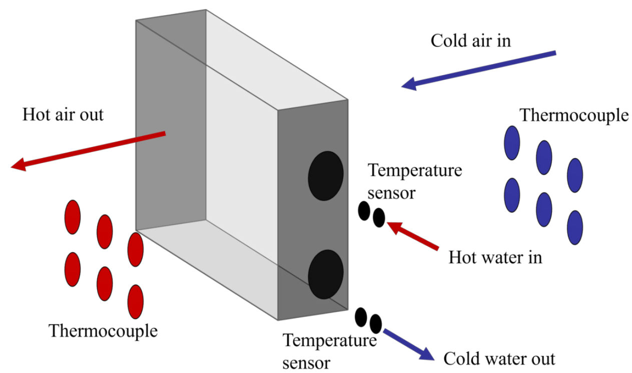

Fig. 2 Schematic of experimental setup [24].

First, two cases are carried out with an air velocity of 0.36 m / s, one with a steady-state assumption and one without. The purpose of these cases is to assess whether the problem under consideration is steady or unsteady. The grid for the case consists of 2.48 million cells and $y^+ \leq 5$. The grid is particularly refined near the tube and fins to resolve the high-temperature and velocity gradients. A comparison of the air outlet temperature and the simulation times between the unstable solution (after 14 flow times) and the steady case is shown in table 2. Since the difference between the two cases is 0.05%, for computational efficiency, the rest of the calculations in this paper are performed using the steady-state assumption.

Table 2 A comparison between steady and unsteady state analysis for an inlet air velocity of 0.36 m/s

	Steady-state	Unsteady
Simulation time	4 hr 20 min	13 hr 30 min
Air outlet temperature	39.36 ^oC	39.38 ^oC

Figure 3a shows the distribution of the air temperature near the aluminum fin – the air flows from left to right. As can be seen, the air heats up as we move toward the right, indicating the transfer of energy to the cool air. Figure 3b shows the temperature distribution at the outlet cross-sectional plane of the copper tube. Since the air flows from left to right, we see higher temperatures in the clockwise direction in the copper tube as well as water. Energy from water is transferred to the copper tube, where, through conduction, the heat is transferred to the outer surface of the tube. On the outer surface of the tube, heat is either convected away by cold air flowing over it or conducted to the aluminum fins, which in turn, also heat the air away from the copper tubes.

Table 3 summarizes the comparison between outlet air temperatures obtained from steady-state simulations with inlet air velocities of 0.25, 0.36 and 0.46 m/s and experimental measurements. As can be noted from the last column, our computations agree well with the measurements and accurately capture the flow physics and heat transfer mechanisms.

Table 3 Comparison of air temperature at the outlet between experiment [24] and present simulations

Air inlet velocity (m/s)	Air outlet temperature (^oC) [24]	Air outlet temperature (^oC) - Present	Difference (%)
0.25	38.15	39.72	4.1%
0.36	38.07	39.36	3.4%
0.46	37.19	38.88	4.5%

Table 4 Operating conditions and physical properties of air and EGW used in the simulations.

	Air	EGW
Inlet temperature (^oC)	55	80
Inlet velocity/flow rate	67 m/s	11 L/min
Density (kg/m^3)	1.0759	1039.6
Dynamic viscosity ($Pa-s$)	1.98e-5	9.81e-4
Thermal conductivity (W/mK)	0.0282	0.3940
Heat Capacity ($J/kg-K$)	1007.7	3514.0

4. RESULTS

As mentioned before, the purpose of this paper is to describe the development and evaluate the accuracy of the machine-learned turbulence model that is used in the TopOpt algorithm to close equations 2 and 3, specifically, the terms shown in expressions 5 and 6. In this section, we will first describe the generation of data sets to train the GP model, followed by the choice of kernel functions and training in Section 4.2. Finally, Section 4.3 evaluates the accuracy of the model by using the turbulent viscosity predicted by the ML algorithm in a zero-equation CFD calculation versus predictions from two-equation $k-\epsilon$-based "truth data" at testing points. The operating conditions and physical properties of the fluids for all subsequent results presented in this paper are summarized in table 4.

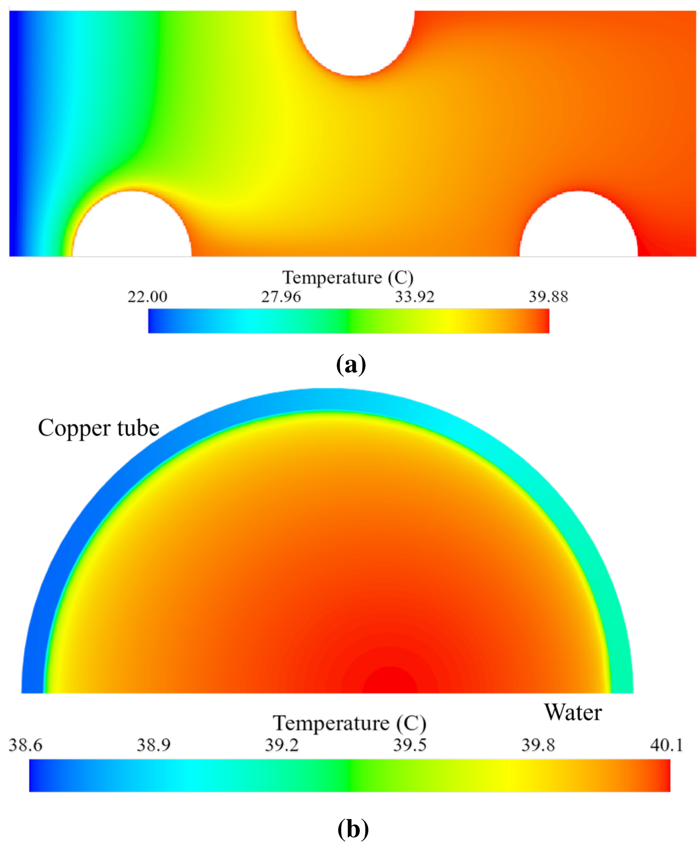

Fig. 3 Distribution of temperatures in (a) air and (b) water for the validation case with air velocity of 0.36 m/s.

4.1 Generation of data for the machine learning model

By varying different constraints, the TopOpt algorithm designed four different types of heat exchangers based on laminar flow conditions, as shown in figure 4. The first design shown in figure 4 (a) was optimized using a design space of 10 in × 10 in × 10 in. The second shown in figure 4 (b) was optimized using half the design space which is then mirrored to produce the entire heat exchanger. Drawing inspiration

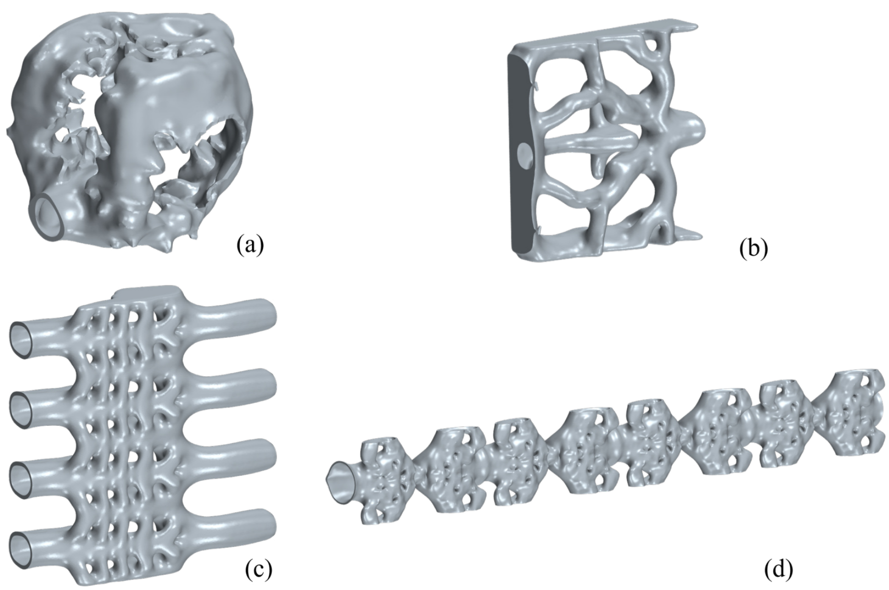

Fig. 4 Types of organic heat exchanger designs, 1-4.

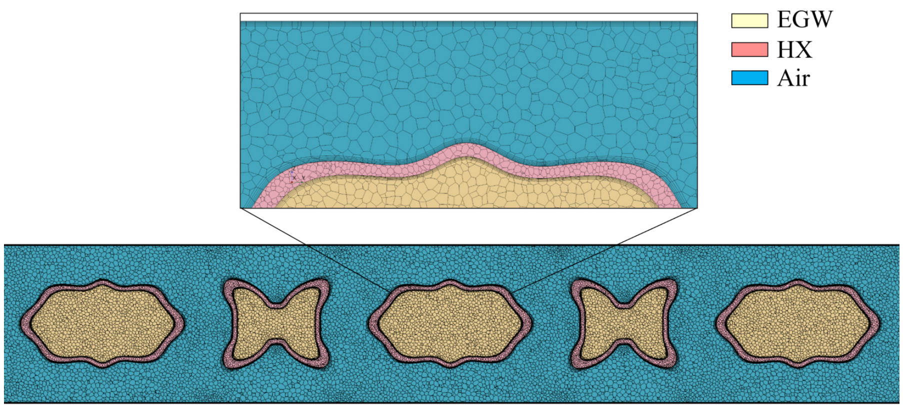

Fig. 5 Meshed domain for design 4.

from conventional heat exchangers, which typically feature multiple identical flow channels, the third design in figure 4 (c) incorporates four flow channels. The optimization for this design type consisted of a domain size 10 in $\times$ 2.5 in $\times$ 1.25 in, equivalent to half of a flow channel. The complete heat exchanger was then generated by duplicating the result eight times. The fourth type of design was a unit cell, the objective function being changed from maximizing the difference between the inlet and outlet EGW temperatures to maximizing the energy density. This unit cell was then replicated 64 times to mirror the same frontal cross-section area as the previous designs. Figure 4 (d) shows the unit cell design applied to a single channel. Further details of the constraints that led to these designs can be found elsewhere [18]. In total, 10 designs belonging to one of these four types were generated. Next, realizable $k-\epsilon$-based calculations were conducted on each of these designs using Star CCM+. The purpose was twofold: (1) to quantify the energy density (heat rejection/wet mass) of each design and (2) to extract spatially averaged turbulent viscosity for each design. To ensure that the velocity and thermal boundary layers were captured, $y^{+}=5$ was maintained for each calculation, an example of which is illustrated in figure 5. For example, the grid used for design 4 consists of 9.73 million cells.

Figures 6 (b), (c) and (d) show the spatial distribution of air temperature, turbulent viscosity, μ_t, and gas-phase

Table 5 Energy densities of designs shown in figure 4.

Design	Energy (kW/lbs)	Density
conventional	0.7	
1	0.24	
2	0.37	
3	1.66	
4	2.82	

Table 6 Comparison between true value and predicted value

True Value	Predicted Value	Error
0.0243	0.0240	1.26 %
0.0155	0.0144	6.9 %

velocity fields, respectively, for design 4. The spatially averaged μ_t is the variable of interest for the machine-learned model. Table 5 summarizes the energy densities, $Q = \dot{m}c_p(T_{in} - T_{out})$ of the four representative designs shown in figure 4. A total of ten designs were evaluated using this methodology and spatially averaged turbulent viscosity is extracted for each design.

4.2 ML Training

In general, in any machine learning algorithm, one or more inputs yield an output. In the current scenario, the TopOpt algorithm requires the turbulent viscosity value as it iterates to generate the design. Among many inputs that could be used, we chose the surface density, defined as the ratio of the outer surface area to the volume occupied by the heat exchanger, as the representative of the geometry as the input to the ML algorithm. As mentioned in the previous paragraph, the turbulent viscosity and surface densities were collected for each design.

Given this, the problem statement becomes: predict the turbulent viscosity given an area density. Note that our data set is limited to 10 points, which is not conducive to neural network-based machine learning algorithms that require hundreds, if not thousands, of data points. However, it is well known in the literature that Gaussian processes work well with smaller datasets [21], which was chosen for the current work. Of the ten designs, eight were used to train the model and the remaining two were used as testing points. In this GP model, the kernel was defined by $(k1 + k2 + k3) * k4$, where $k1$ to $k4$ correspond to spline, linear, periodic, and Brownian, respectively. Figure 7 shows the result of the trained algorithm. The vertical axis is the turbulent viscosity and the horizontal axis is the surface density.

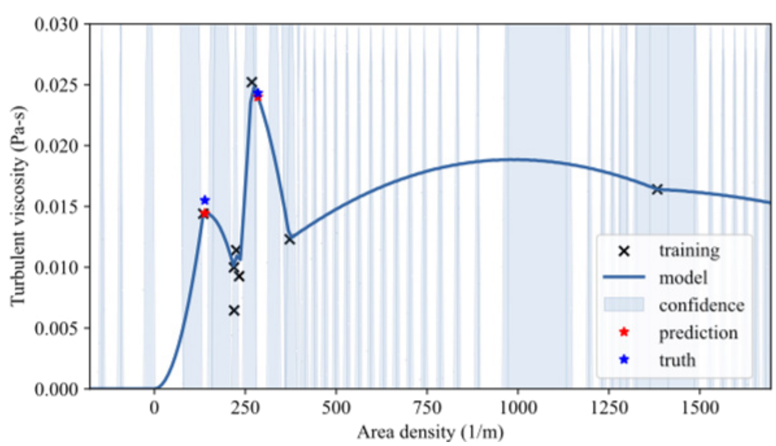

Fig. 7 GP model predicting μ_t as a function of area density.

Table 6 shows the comparison between the true value and the predicted value by the model for the two testing points (shown in red in figure 7). For the given limited training data size, the model predicts turbulent viscosity with good accuracy. The GP model was then incorporated into the topology optimization code which could now incorporate turbulence

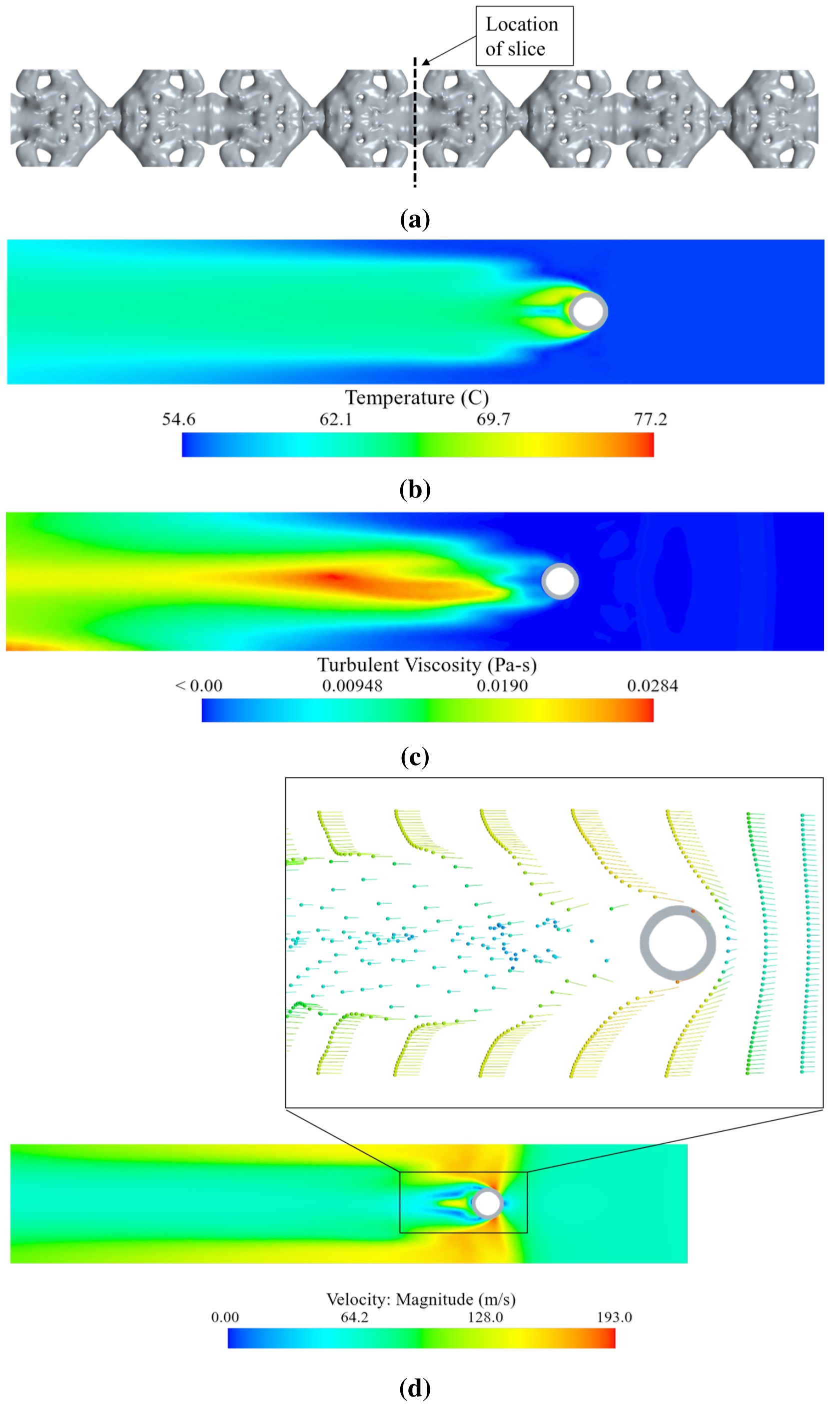

Fig. 6 Spatial distribution of (b) air temperature, (c) turbulent viscosity and (d) velocity at the mid-section plane shown in (a).

Table 7 Comparison of coolant and air outlet temperatures between the truth and GP-based models.

	$k-\epsilon$ model	GP Model	Difference (%)
Air outlet (^oC)	56.53	57.00	0.83
EGW Outlet 1 (^oC)	65.25	65.02	0.35
EGW Outlet 2 (^oC)	66.29	66.18	0.16
EGW Outlet 3 (^oC)	67.13	67.16	0.04
EGW Outlet 4 (^oC)	68.34	68.06	0.41

to resemble true conditions for the design space.

4.3 Model Validation

To validate the GP model, we conducted two simulations on a test design shown in figure 4 (c), one using the realizable $k-\epsilon$ model that is treated as the "truth" data and the other using a zero-equation model where the turbulent viscosity was predicted by the ML model based on the area density of the test design. There are some challenges in incorporating a zero equation model to resolve complex turbulent flow features. However, one must consider the convergence criteria of the TopOpt algorithm and the fact that the complexity increases as we add more PDE's to solve for each successive iteration of the process. Table 7 shows a comparison of the temperatures at the four EGW outlets and the air outlet between the "truth" ($k-\epsilon$) and the GP-informed zero-equation predictions, showing excellent agreement. The corresponding temperature distribution is shown in figure 8. Here, a loss of information is evident; however, the flow structures are qualitatively similar.

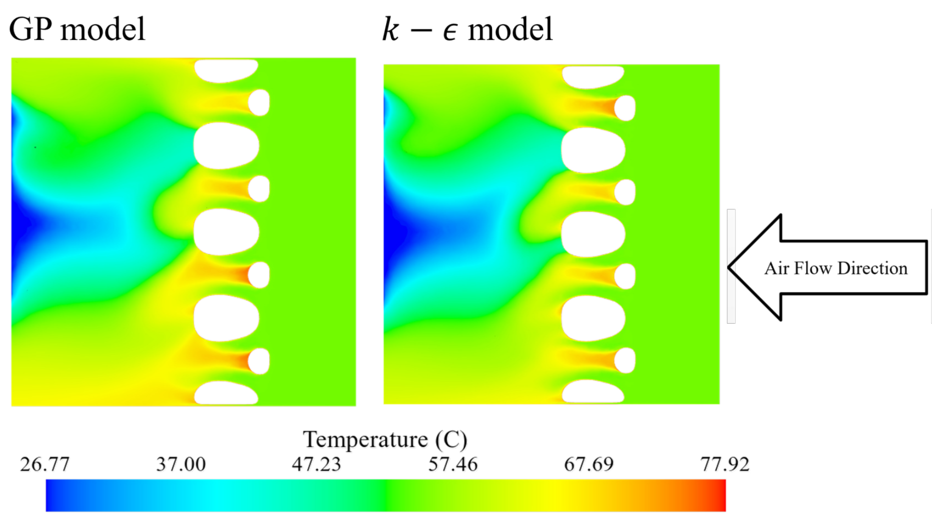

Fig. 8 Temperature distribution in the air domain at the mid-section plane.

5. CONCLUSIONS

In this study, a machine-learned turbulence model was developed to predict turbulent viscosity as a function of area density for complex geometries. Given the size of the data set $\mathcal{O}(10)$, it was determined that Gaussian Processes would be the most appropriate model for this purpose. An experimental validation study was conducted to show that the relevant flow features and mechanisms from conjugate heat transfer were captured and that the simulations showed good agreement with the experimental results. Heat exchanger designs were generated using topology optimization algorithms assuming laminar flow. The designs were evaluated under turbulent flow conditions using the realizable $k-\epsilon$ model. The Gaussian Process model designed from the aforementioned training data was evaluated using the zero equation turbulence model to determine the accuracy of the machine-learned algorithm. Compared to the test data, the GP model showed good agreement. The algorithm was incorporated into the topology optimization code to generate designs of heat exchangers that represent real operating conditions.

ACKNOWLEDGMENTS

This work is supported by Eaton Corporation via the US Army Engineer Research and Development Center (ERDC) grant number W912HZ-21-BAA-01.

REFERENCES

[1] Ramesh K Shah and Dusan P Sekulic. *Fundamentals of heat exchanger design*. John Wiley & Sons, 2003.

[2] Ali Sadeghianjahromi and Chi-Chuan Wang. Heat transfer enhancement in fin-and-tube heat exchangers – a review on different mechanisms. *Renewable and Sustainable Energy Reviews*, 137:110470, 2021.

[3] Ashish J. Modi and Manish K. Rathod. Comparative study of heat transfer enhancement and pressure drop for fin-and-circular tube compact heat exchangers with sinusoidal wavy and elliptical curved rectangular winglet vortex generator. *International Journal of Heat and Mass Transfer*, 141:310–326, 2019.

[4] Haijun Wang, Ting Fu, Jiangbo Wang, Feng Zhang, Kan Zhang, and Xiaolei Deng. Study on heat transfer performance of fin-and-tube heat exchanger with elliptical fins. *Journal of Energy Storage*, 56:105956, 2022.

[5] Parinya Pongsoi, Santi Pikulkajorn, Chi-Chuan Wang, and Somchai Wongwises. Effect of number of tube rows on the air-side performance of crimped spiral fin-and-tube heat exchanger with a multipass parallel and counter cross-flow configuration. *International Journal of Heat and Mass Transfer*, 55(4):1403–1411, 2012.

[6] Turo Välikangas, Mikko Folkersma, Miikka Dal Maso, Tuomo Keskitalo, Petteri Peltonen, and Ville Vuorinen. Parametric cfd study for finding the optimal tube arrangement of a fin-and-tube heat exchanger with plain fins in a marine environment. *Applied Thermal Engineering*, 200:117642, 2022.

[7] Ahmad Fawaz, Yuchao Hua, Steven Le Corre, Yilin Fan, and Lingai Luo. Topology optimization of heat exchangers: A review. *Energy*, 252:124053, 2022.

[8] Lukas Christian Høghøj, Daniel Ruberg Nørhave, Joe Alexandersen, Ole Sigmund, and Casper Schousboe Andreasen. Topology optimization of two fluid heat exchangers. *International Journal of Heat and Mass Transfer*, 163:120543, 2020.

[9] Hiroki Kobayashi, Kentaro Yaji, Shintaro Yamasaki, and Kikuo Fujita. Topology design of two-fluid heat exchange. *Structural and Multidisciplinary Optimization*, 63:821–834, 2021.

[10] Talib Dbouk. A review about the engineering design of optimal heat transfer systems using topology optimization. *Applied Thermal Engineering*, 112:841–854, 2017.

[11] Mark Christian E Manuel and Po Ting Lin. Heat exchanger design with topology optimization. *Heat Exchangers-Design, Experiment and Simulation*, page 14, 2017.

[12] Sumer B Dilgen, Cetin B Dilgen, David R Fuhrman, Ole Sigmund, and Boyan S Lazarov. Density based topology optimization of turbulent flow heat transfer systems. *Structural and Multidisciplinary Optimization*, 57:1905–1918, 2018.

[13] Himakar Ganti, Luis Bravo, and Prashant Khare. Interactions between high hydrogen content syngas–air premixed flames and homogeneous isotropic turbulence: Flame thickening. *Physics of Fluids*, 35(7):075150, 2023.

[14] Manu Kamin and Prashant Khare. The effect of weber number on spray and vaporization characteristics of liquid jets injected in air crossflow. *Journal of Fluids Engineering*, 144(6):061108, 2022.

[15] Hua-Guang Li, Prashant Khare, Hong-Gye Sung, and Vigor Yang. A large-eddy-simulation study of combustion dynamics of bluff-body stabilized flames. *Combustion Science and Technology*, 188(6):924–952, 2016.

[16] Manu Kamin, James Eblin, and Prashant Khare. The nexgen burner: Non-reacting gaseous and spray dynamics. *Physics of Fluids*, 35(11), 2023.

[17] S. B. Pope. *Turbulent flows*. Cambridge University Press, Cambridge;New York;, 2000.

[18] Botao Zhang, Vysakh Venugopal, Mitansh Tripathi, Navaneeth Chandran, Niloofar Sanaei, Logan Ware, Prashant Khare, and Sam Anand. Design for additive manufacturing constrained topology optimization of liquid-to-air heat exchangers with ml-based turbulent flow considerations. In *Proceedings of the ASME 2024 19th International Manufacturing Science and Engineering Conference, MSEC2024 (to appear)*, number MSEC2024-122417, Knoxville, Tennessee, June 2024. ASME.

[19] David C. Wilcox. *Turbulence modeling for CFD*. DCW Industries, La Canada, Calif, 2nd edition, 2002.

[20] Tsan-Hsing Shih, William W. Liou, Aamir Shabbir, Zhigang Yang, and Jiang Zhu. A new $k - \epsilon$ eddy viscosity model for high reynolds number turbulent flows. *Computers & Fluids*, 24(3):227–238, 1995.

[21] Carl E. Rasmussen and Christopher K. I. Williams. *Gaussian processes for machine learning*. MIT Press, 2006.

[22] Himakar Ganti, Manu Kamin, and Prashant Khare. Design space exploration of turbulent multiphase flows using machine learning-based surrogate model. *Energies*, 13(17):4565, 2020.

[23] Himakar Ganti and Prashant Khare. Data-driven surrogate modeling of multiphase flows using machine learning techniques. *Computers & Fluids*, 211:104626, 2020.

[24] Josip Batista, Anica Trp, and Kristian Lenic. Experimentally validated numerical modeling of heat transfer in crossflow air-to-water fin-and-tube heat exchanger. *Applied Thermal Engineering*, 212:118528, 2022.